MDM2 acts as a timer reporting the length of mitosis

Luke J. Fulcher, Tomoaki Sobajima, Ian Gibbs-Seymour, and Francis A. Barr*

Affiliations:

Department of Biochemistry, University of Oxford, South Parks Road, Oxford OX1 3QU.

*Corresponding author. Email: francis.barr@bioch.ox.ac.uk

Abstract:

Delays in mitosis trigger a p53-dependent arrest in G1 of the following cell cycle, enabling cells to react to changes promoting aneuploidy [1-10]. How delays in mitosis are sensed and result in cells becoming arrested in the subsequent G1 phase is unclear. We have identified MDM2, the p53 ubiquitin ligase, as the key molecular timer that enables cells to respond to defects in mitosis by arresting in the subsequent G1. We demonstrate that MDM2 has a short half-life and ongoing protein synthesis is therefore necessary to maintain its steady-state concentration. Because protein synthesis is attenuated in mitosis, the amount of MDM2 falls during mitosis but remains above a crucial threshold for p53 regulation at the onset of G1. However, when mitosis is prolonged and the amount of MDM2 drops below this threshold level, p53 is stabilised in new G1 cells, triggering increased p21 synthesis and cell cycle arrest. Our findings shed light on how abrogation of this process enables p53 mutant cancer cells to bypass the key regulation that senses and responds to aneuploidy in normal cells.

Main text:

We hypothesized that the detection of delays in mitosis is linked to a biochemical reaction consuming a key regulatory component of the p53 pathway, which thus acts as a timer reporting the length of mitosis (Fig. 1a). This led us to consider the role of MDM2, the p53 E3 ubiquitin-ligase [11-13]. In interphase cells, the levels of p53 are regulated by ongoing synthesis and proteasomal destruction triggered by the MDM2 E3 ubiquitin-ligase (Fig. 1b). DNA damage and other stress signals mediated by conserved signalling pathways inhibit MDM2 activity towards p53 [14]. This results in p53 stabilization, an increase in the steady-state concentration of p53, and p53-dependent transcription of DNA repair proteins, cell cycle regulators such as the CDK-inhibitor p21, and, if DNA damage is not repaired, pro-apoptotic factors [14]. Like p53, MDM2 stability is tightly regulated. MDM2 has a short half-life and is subject to autoubiquitination or ubiquitination by other E3 ubiquitin-ligases [15, 16]. We inferred that entry into mitosis would have important functional consequences for both MDM2 itself and MDM2 regulation of p53 at the onset of the following G1 phase. Upon entry into mitosis there is a strong general attenuation of both transcription and translation until cells exit mitosis and re-enter G1, when transcription and protein synthesis resume [17-19]. Thus, MDM2 synthesis will stop or become greatly reduced following mitotic entry, whereas its turnover will continue due to ongoing autoubiquitination or ubiquitination by other E3 ubiquitin-ligases. For normal length mitoses, early G1 cells will retain sufficient MDM2 to regulate p53 normally and prevent p21-induced cell cycle arrest. If mitosis is prolonged and MDM2 concentration falls below this threshold, p53 stabilization early in the following G1 will result in a p21-dependent cell cycle arrest. Our hypothesis is that these are general properties of the MDM2-p53 pathway, and provide a mechanism to monitor the length of mitosis, independent from the cause of the delay. While elements of this hypothesis have been discussed previously [20, 21], to date there is no experimental evidence in support of this proposal. We therefore set out to test these ideas and whether MDM2 has the hallmarks predicted for the mitotic timer protein.

First, we measured the stability of MDM2 in untransformed diploid telomerase-immortalised retinal pigmented epithelium (hTERT-RPE1) cells with wild-type p53, and a range of transformed human cancer cell lines, in both interphase and mitotic states. MDM2 and p53 expression was confirmed for all cell lines in asynchronous culture (Fig. S1a). HeLa cells have much lower levels of MDM2 and p53

than other cell lines due to expression of the HPV E6 protein which targets p53 for destruction, and because MDM2 is a transcriptional target of p53 [22, 23]. We then arrested these different cell lines in mitosis with two different anti-mitotic agents (nocodazole or the Eg5 kinesin inhibitor STLC) and measured the amount of MDM2 by Western blotting. These approaches revealed that MDM2 falls to very low levels during an 18 h mitotic arrest in all cell lines, regardless of which agent was used to trigger the arrest (Fig. 1c, S1b and S1c). In contrast, p53 was stable in a prolonged mitotic arrest in all cell lines except HeLa, consistent with the idea that its destruction requires MDM2 (Fig. S1b). Compared to the other cell lines, HeLa cells had very low levels of p53 initially due to HPV E6 expression, which fell below the detection limit in the mitotic arrest samples (Fig. S1b). This decrease in MDM2 was dependent on the length of time in mitosis, showing a robust decrease from 1 to 4 h of mitotic delay with an estimated half-life for MDM2 of ~26 min (Fig. 1d). Addition of the proteasome inhibitor MG132 prevented MDM2 destruction after 4 h of mitotic delay (Fig. 1e). Thus, global inhibition of protein synthesis combined with its short half-life, can explain how the amount of MDM2 decreases in mitotic cells by a ubiquitination-dependent pathway.

For further functional experiments, we first established that hTERT-RPE1 cells provided a suitable experimental model for testing the mitotic timer response. In these experiments we activated the spindle checkpoint for 1, 4 or 18 h by the addition of a low dose of 25 ng/ml (83 nM) nocodazole (Fig. S1d), harvested the mitotic cells, then replated them in fresh growth medium lacking nocodazole and test for synchronous exit from mitosis and proliferation (Fig. S1e). In this assay, prolonging mitosis for 4 or 18h by activating the spindle checkpoint resulted in cell cycle arrest and a cessation of cell proliferation in hTERT-RPE1 $p53^{WT}$ cells (Fig. 1f). Delaying cells in mitosis for 1h had little effect on their proliferation (Fig. 1f), suggesting that in this situation MDM2 remains above the threshold level to trigger G1 arrest. An hTERT-RPE1 $p53^{KO}$ cell line showed normal proliferation after 1, 4 or 18 h mitotic delay (Fig. 1f), confirming the cell cycle arrest is due to a p53-dependent pathway. Crucially, the amount of MDM2 measured by Western blotting correlated with the reduction in cell proliferation, showing a partial reduction after 1 h mitotic delay, and near complete loss at 4 h and 18 h of delay (Fig. 1c and 1d). This behaviour is consistent with the idea that MDM2 acts as a timer for the length of mitosis, and cell cycle arrest is triggered in the following G1 when its concentration falls below a threshold level.

The mechanism of MDM2 turnover in mitosis is a critical component of this proposed function. As already shown, this is likely to be via a ubiquitination-dependent pathway (Fig. 1e). We favour an auto-ubiquitination mechanism (Fig. 2a), since this would make the rate of MDM2 turnover less dependent on other factors including MDM2 concentration, assuming that the availability of charged E2-ubiquitin conjugates is not limiting. Using cycloheximide to block new protein synthesis, we found that endogenous MDM2 has a half-life of ~30 minutes in all of the cell lines tested, except HeLa where it is shorter due to the presence of HPV E6 (Fig. 2b and S2). To investigate this potential auto-ubiquitination mechanism, we asked which domains of MDM2 are required for its turnover. Using cycloheximide to inhibit protein synthesis, we have mapped MDM2 turnover to the C-terminal RING domain responsible for E3-ubiquitin ligase activity towards p53 (Fig. 2c). Using published structure-function data we have made specific I440A and R479A point mutants on the surface of the RING domain that prevent E2-ubiquitin binding but do not alter the structure [24]. These mutants show stabilization compared to wild-type MDM2 (Fig. 2c). Combined depletion of UBE2D2 and UBE2D3, the MDM2 E2 enzymes resulted in pronounced increase in the amount of MDM2 and stabilisation of MDM2 when protein synthesis was inhibited (Fig. 2d). Moreover, inhibition of the proteasome stabilises MDM2 and resulting in a rise of concentration over time (Fig. 2e). It was also important to establish whether the two major cell cycle ubiquitin ligases associated with mitosis, the anaphase promoting complex/cyclosome (APC/C) and Skp1-Cullin-F-box (SCF) play a role in MDM2 turnover [25]. MDM2 turnover was not prevented by depletion of either the APC/C co-activator cell division cycle 20 homologue (CDC20) or β-transducin-repeat containing protein 1 (β-TrCP1), a major substrate binding subunit for SCF, or addition of the APC/C inhibitor proTAME (Fig. S3a-S3c).

100 Together, these results provide support for the notion that MDM2 stability in mitosis is controlled by
101 auto-ubiquitination, rather than the canonical cell cycle ubiquitin-ligases.

102 Testing the proposed mitotic timer mechanism is complicated, since removal or manipulation of
103 MDM2 activity using standard genetic methods will cause p53 stabilization and cell cycle arrest
104 independent from mitosis. We therefore needed to specifically target MDM2 within mitosis, and
105 uncouple its stability from the length of time spent in mitosis. To selectively modulate MDM2
106 stability, we used the MDM2 PROteolysis-TArgeting Chimera (PROTAC) reagent MD-224 [26], which
107 combines the MDM2-binding drug Nutlin-3a with a ligand for the Cereblon-Cullin 4A-Rbx1 E3
108 ubiquitin-ligase (Fig. S4a). In asynchronous cultures of hTERT-RPE1 p53^{WT} cells we observed that MD-
109 224 causes rapid proteasome-dependent destruction of MDM2, and that its removal resulted in
110 rapid re-accumulation of MDM2 (Fig. S4b and S4c). The latter result is important since we need to
111 add MD-224 in mitosis, then wash it out before cells exit mitosis and enter G1. Confirming the
112 anticipated functional consequences of MDM2 destruction under these conditions, we observed p53
113 stabilisation, and after a short delay, an increase in p21 during the MD-224 washout period (Fig.
114 S4b). In hTERT-RPE1 p53^{KO} cells, MD-224 resulted in rapid MDM2 destruction, but the amount of
115 MDM2 did not recover rapidly once MD-224 was washed out (Fig. S4b), since MDM2, like p21, is a
116 transcriptional target of p53 [23]. Importantly, we confirmed that MD-224 is also active in cells
117 arrested in mitosis, and leads to rapid MDM2 destruction within 1 h in both hTERT-RPE1 p53^{WT} and
118 p53^{KO} cells (Fig. S4d). Compared to asynchronous cell cultures where most cells are in G1, S or G2
119 phase, the amount of MDM2 was reduced even with 1 h mitotic delay in the absence of MD-224
120 (Fig. S4d and S4e), in agreement with the results in Figure 1 showing loss of MDM2 in prolonged
121 mitosis. As expected, given the mode of action of MD-224, MDM2 destruction was prevented when
122 the mitotic cells were pre-incubated with the proteasome inhibitor MG132 (Fig. S4e).

123 These results enabled us to test the idea that the stability of MDM2 is a key component of the
124 mitotic timer. For this purpose, we combined a short 1 h or long 4 h spindle checkpoint arrest with
125 MD-224 to destabilise MDM2 in hTERT-RPE1 p53^{WT} and p53^{KO} cells (Fig. 3a). Biochemical analysis of
126 these cells confirmed that MDM2 was still present after a 1 h mitotic delay, albeit reduced in
127 amount (Fig. 3b, lanes 1 and 9; Fig. 3c), but was further reduced to undetectable levels when MD-
128 224 was added during that 1 h delay (Fig. 3b, lanes 1 and 2; Fig. 3c). After a 4 h delay, MDM2 was
129 strongly reduced even in the absence of MD-224, and was further reduced to undetectable levels if
130 MD-224 was present (Fig. 3b, lanes 5 and 6). In p53^{WT} cells, p53 and p21 significantly increased in the
131 G1 following a 1 h mitotic delay when MDM2 was destabilised in mitosis by MD-224, to the levels
132 seen after a 4 h mitotic delay (Fig. 3b, compare lanes 3- 4 with lanes 7-8; Fig. 3d and 3e). Crucially, a
133 short 1 h mitotic delay in the presence but not the absence of MD-224 triggered a cell cycle arrest
134 and loss of proliferation in p53^{WT} cells (Fig. 3f). A long 4 h mitotic delay triggered a cell cycle arrest
135 and loss of proliferation in both the presence and absence of MD-224 (Fig. 3f), suggesting that after
136 4 hours in mitosis MDM2 concentration had already fallen below the threshold needed to prevent
137 p53 stabilisation and induction of p21. Matching this behaviour, p53 was stabilised in the
138 subsequent G1 phase, leading to upregulation of its transcriptional targets, including MDM2 itself
139 (Fig. 3b, compare lanes 3-4 with 7-8). This behaviour confirmed that MD-224 had been efficiently
140 removed prior to G1 entry, supporting the view that its effects are due to the destabilisation of
141 MDM2 in mitosis. Note that because MDM2 is a transcriptional target of p53 it shows reduced
142 steady-state levels in p53^{KO} cells compared to p53^{WT} cells (Fig. 3b, lane 9, AS p53^{WT} and p53^{KO}).
143 Confirming the dependence on p53 for the G1 arrest, induction of p21 and reduced cell proliferation
144 were not observed with hTERT-RPE1 p53^{KO} cells for any of these conditions (Fig. 3b and 3e-3f). Taken
145 together, our data demonstrate that the amount of MDM2 remaining at the end of mitosis is an
146 important factor in determining whether cells undergo p53-dependent arrest following delayed cell
147 division.

148 Next, the cell cycle path taken by cells undergoing normal length or delayed mitosis in the presence
149 and absence of MD-224 was analysed. Single cell tracing of hTERT-RPE1 p53^{WT} FUCCI cells was used
150 to follow mitotic exit, the length of G1 and entry into S phase (Fig. S5a and S5b) [27]. For these

experiments, mitotic cells were tracked from asynchronous cultures (no delay), or after washout following a short or long mitotic delay. Unperturbed cells ($AS^{No\ delay}$ in Fig. S5c and S5d) and cells delayed in mitosis for a short period showed a similar G1 duration of 9.5-9.7 h ± 3.5 h (Noc^{Short} in Fig. 4a and 4b). However, even a short delay in mitosis increased the proportion of cells arrested in G1 for at least 20 h from 8% (Fig. S5d, $AS^{NoDelay}$) to 52% (Fig. 4a, Noc^{Short}). Conversely, shortening this delay by addition of an MPS1 inhibitor (Noc^{Short} + MPS1i) to collapse the spindle checkpoint, prevented the increase in cells arresting in G1 from 52% to 21%, and reduced G1 length in cells entering S phase to 8.9 h ± 3.1 h, slightly below the duration observed in the unperturbed cells ($AS^{No\ delay}$), despite the presence of chromosome segregation defects (Fig. S5c-S5e). Thus, the proportion of cells undergoing a G1 arrest and length of G1 correlate with the increased length of time in mitosis, rather than with chromosome mis-segregation events. In comparison, a long mitotic delay (Noc^{Long}) resulted in over 94% G1 arrest, and the length of G1 in cells entering S phase increased to 13.3 h ± 6.0 h. Most importantly, addition of 100 nM MD-224 during the short mitotic delay (Noc^{Short} +MD-224) resulted in over 99% arrest in G1, with very few cells entering S phase after a prolonged time >20 h in G1 (Fig. 4a and 4b). In all cases the G1 arrest was robust and maintained for at least 60 h, the maximum time imaged in these experiments. This G1 arrest was not observed in hTERT-RPE1 $p53^{KO}$ FUCCI cells for either the long mitotic arrest (Noc^{Long}) (Fig. 4a and 4b) or when MD-224 was added during a short mitotic arrest (Noc^{Short} +MD-224) (Fig. 4a and 4b). Furthermore, treatment of mitotic cells in asynchronous cultures with Nutlin-3A, an MD-224 related compound which blocks the MDM2-p53 interaction but does not trigger MDM2 destruction, did not result in extended G1 or cell cycle arrest in the following G1 (Fig. S5d, compare $AS^{NoDelay}$ with Nutlin-$3A^{NoDelay}$). Under the same conditions, MD-224 resulted in an extension of G1 from 9.7 ± 3.5 h to 14.8 ± 2.4 h, and increased the level of G1 arrested cells from 8% to 51% (Fig. S5d, compare $AS^{NoDelay}$ with MD-$224^{NoDelay}$). Similarly, treatment of cells in S and G2 with MD-224 did not trigger arrest in G1 phase of the following cell cycle and all cells entered S phase, although we did observe a lengthened G1 phase (Fig. S5f). This is consistent with our data showing rapid recovery of MDM2 following washout of MD-224 in asynchronous cell cultures (Fig. S4b). To determine the precise threshold for MDM2, we titrated MD-224 and measured the amount of MDM2 by Western blotting, and cell cycle arrest using the hTERT-RPE1 $p53^{WT}$ FUCCI cell line. This revealed a sharp threshold for the G1 arrest, closely correlating with the level of p21 and mirroring the behaviour of MDM2 (Fig. 4c). The 100 nM concentration of MD-224 used for other experiments sits at the top of this sigmoidal curve explaining its potency. Under conditions where mitosis is delayed for a short period, the level of p21 rises only slightly in early G1 cells, whereas when 100 nM MD-224 is added during the short mitotic delay then removed, p21 levels rise sharply, plateau and are then maintained into late G1 (Fig. 4d). We conclude that p53 and p21 dependent G1 arrest following delayed mitosis is triggered by reduction of MDM2 below a threshold concentration in mitosis where re-synthesis of the protein is not possible (Fig. 4e).

Delayed progression through mitosis caused by chromosome instability, aneuploidy, the removal of centrosomes, or anti-mitotic drugs targeting the microtubule cytoskeleton results in a p53 and p21 dependent cell cycle arrest in G1 following the perturbed mitosis [1-6]. This response is lost in cancer cells in which p53 has become inactivated by mutation or other mechanisms including expression of viral oncoproteins [7-10]. Crucially, G1 cell cycle arrest following prolonged mitosis occurs even in the absence of detectable DNA damage [1-10]. Our work supports the idea that MDM2, due to its short half-life, is the key timer component in the mechanism that triggers a robust cell cycle arrest in the G1 phase following a prolonged delay in mitosis [20, 21]. This provides an explanation for p53-dependent, yet DNA damage signalling-independent cell cycle arrest in G1 following delays in mitosis. Loss of function mutations or deletion of p53 are amongst the most common genetic changes associated with aneuploid cancers, and we propose this is in part due to the mitotic timer effect. Highly aneuploid tumour cells often show prolonged mitosis due to extended spindle assembly checkpoint activation caused by mitotic defects [1-10]. As long as wild-type p53 functionality is present, the mechanism we have described here will channel these cells into a

prolonged cell cycle arrest in the following G1. By contrast, loss of this protective response enables aneuploid cells to continue proliferating. These findings shed new light on to the functions of MDM2 and have potentially important consequences for our understanding of how aneuploidy is detected in normal cells, and how failure of this process facilitates genome instability and unchecked proliferation in cancers.

Acknowledgments: We thank Prof. Ulrike Grüneberg and our colleagues in the Barr group for discussion and advice, and Dr. Martin Attwood for help with generation and validation of the p53^{KO} hTERT-RPE1 cells.

Funding: Cancer Research UK program grant award C20079/A24743 (FAB), and Cancer Research UK Career Development Fellowship C62538/A24670 (IGS).

Author contributions: Conceptualization: FAB; Methodology: LJF, TS, IGS, FAB; Investigation: LJF, TS; Funding acquisition: FAB, IGS; Supervision: FAB; Writing – original draft: FAB; Writing – review and editing: FAB, LJF, TS

Competing interests: Authors declare that they have no competing interests.

Data and materials availability: All data are available in the main text or the supplementary materials. Cell lines and other materials generated in this study can be obtained by writing to the corresponding author.

References

1. Wong, Y.L., et al., *Cell biology. Reversible centriole depletion with an inhibitor of Polo-like kinase 4.* Science, 2015. **348**(6239): p. 1155-60.
2. Thompson, S.L. and D.A. Compton, *Proliferation of aneuploid human cells is limited by a p53-dependent mechanism.* J Cell Biol, 2010. **188**(3): p. 369-81.
3. Li, R. and J. Zhu, *Effects of aneuploidy on cell behaviour and function.* Nat Rev Mol Cell Biol, 2022. **23**(4): p. 250-265.
4. Thompson, S.L. and D.A. Compton, *Examining the link between chromosomal instability and aneuploidy in human cells.* J Cell Biol, 2008. **180**(4): p. 665-72.
5. Uetake, Y. and G. Sluder, *Prolonged prometaphase blocks daughter cell proliferation despite normal completion of mitosis.* Curr Biol, 2010. **20**(18): p. 1666-71.
6. Yang, Z., et al., *Extra centrosomes and/or chromosomes prolong mitosis in human cells.* Nat Cell Biol, 2008. **10**(6): p. 748-51.
7. Lambrus, B.G., et al., *A USP28-53BP1-p53-p21 signaling axis arrests growth after centrosome loss or prolonged mitosis.* J Cell Biol, 2016. **214**(2): p. 143-53.
8. Meitinger, F., et al., *53BP1 and USP28 mediate p53 activation and G1 arrest after centrosome loss or extended mitotic duration.* J Cell Biol, 2016. **214**(2): p. 155-66.
9. Cuella-Martin, R., et al., *53BP1 Integrates DNA Repair and p53-Dependent Cell Fate Decisions via Distinct Mechanisms.* Mol Cell, 2016. **64**(1): p. 51-64.
10. Fong, C.S., et al., *53BP1 and USP28 mediate p53-dependent cell cycle arrest in response to centrosome loss and prolonged mitosis.* Elife, 2016. **5**.
11. Kubbutat, M.H., S.N. Jones, and K.H. Vousden, *Regulation of p53 stability by Mdm2.* Nature, 1997. **387**(6630): p. 299-303.
12. Haupt, Y., et al., *Mdm2 promotes the rapid degradation of p53.* Nature, 1997. **387**(6630): p. 296-9.
13. Honda, R., H. Tanaka, and H. Yasuda, *Oncoprotein MDM2 is a ubiquitin ligase E3 for tumor suppressor p53.* FEBS Lett, 1997. **420**(1): p. 25-7.
14. Blackford, A.N. and S.P. Jackson, *ATM, ATR, and DNA-PK: The Trinity at the Heart of the DNA Damage Response.* Mol Cell, 2017. **66**(6): p. 801-817.

15. Fang, S., et al., *Mdm2 is a RING finger-dependent ubiquitin protein ligase for itself and p53.* J Biol Chem, 2000. **275**(12): p. 8945-51.
16. Inuzuka, H., et al., *Phosphorylation by casein kinase I promotes the turnover of the Mdm2 oncoprotein via the SCF(beta-TRCP) ubiquitin ligase.* Cancer Cell, 2010. **18**(2): p. 147-59.
17. Fan, H. and S. Penman, *Regulation of protein synthesis in mammalian cells. II. Inhibition of protein synthesis at the level of initiation during mitosis.* J Mol Biol, 1970. **50**(3): p. 655-70.
18. Taylor, J.H., *Nucleic acid synthesis in relation to the cell division cycle.* Ann N Y Acad Sci, 1960. **90**: p. 409-21.
19. Prescott, D.M. and M.A. Bender, *Synthesis of RNA and protein during mitosis in mammalian tissue culture cells.* Exp Cell Res, 1962. **26**: p. 260-8.
20. Blagosklonny, M.V., *Prolonged mitosis versus tetraploid checkpoint: how p53 measures the duration of mitosis.* Cell Cycle, 2006. **5**(9): p. 971-5.
21. Santaguida, S. and A. Amon, *Short- and long-term effects of chromosome mis-segregation and aneuploidy.* Nat Rev Mol Cell Biol, 2015. **16**(8): p. 473-85.
22. Scheffner, M., et al., *The HPV-16 E6 and E6-AP complex functions as a ubiquitin-protein ligase in the ubiquitination of p53.* Cell, 1993. **75**(3): p. 495-505.
23. Barak, Y., et al., *mdm2 expression is induced by wild type p53 activity.* EMBO J, 1993. **12**(2): p. 461-8.
24. Nomura, K., et al., *Structural analysis of MDM2 RING separates degradation from regulation of p53 transcription activity.* Nat Struct Mol Biol, 2017. **24**(7): p. 578-587.
25. Nakayama, K.I. and K. Nakayama, *Ubiquitin ligases: cell-cycle control and cancer.* Nat Rev Cancer, 2006. **6**(5): p. 369-81.
26. Li, Y., et al., *Discovery of MD-224 as a First-in-Class, Highly Potent, and Efficacious Proteolysis Targeting Chimera Murine Double Minute 2 Degrader Capable of Achieving Complete and Durable Tumor Regression.* J Med Chem, 2019. **62**(2): p. 448-466.
27. Sakaue-Sawano, A., et al., *Visualizing spatiotemporal dynamics of multicellular cell-cycle progression.* Cell, 2008. **132**(3): p. 487-98.

Main Figures

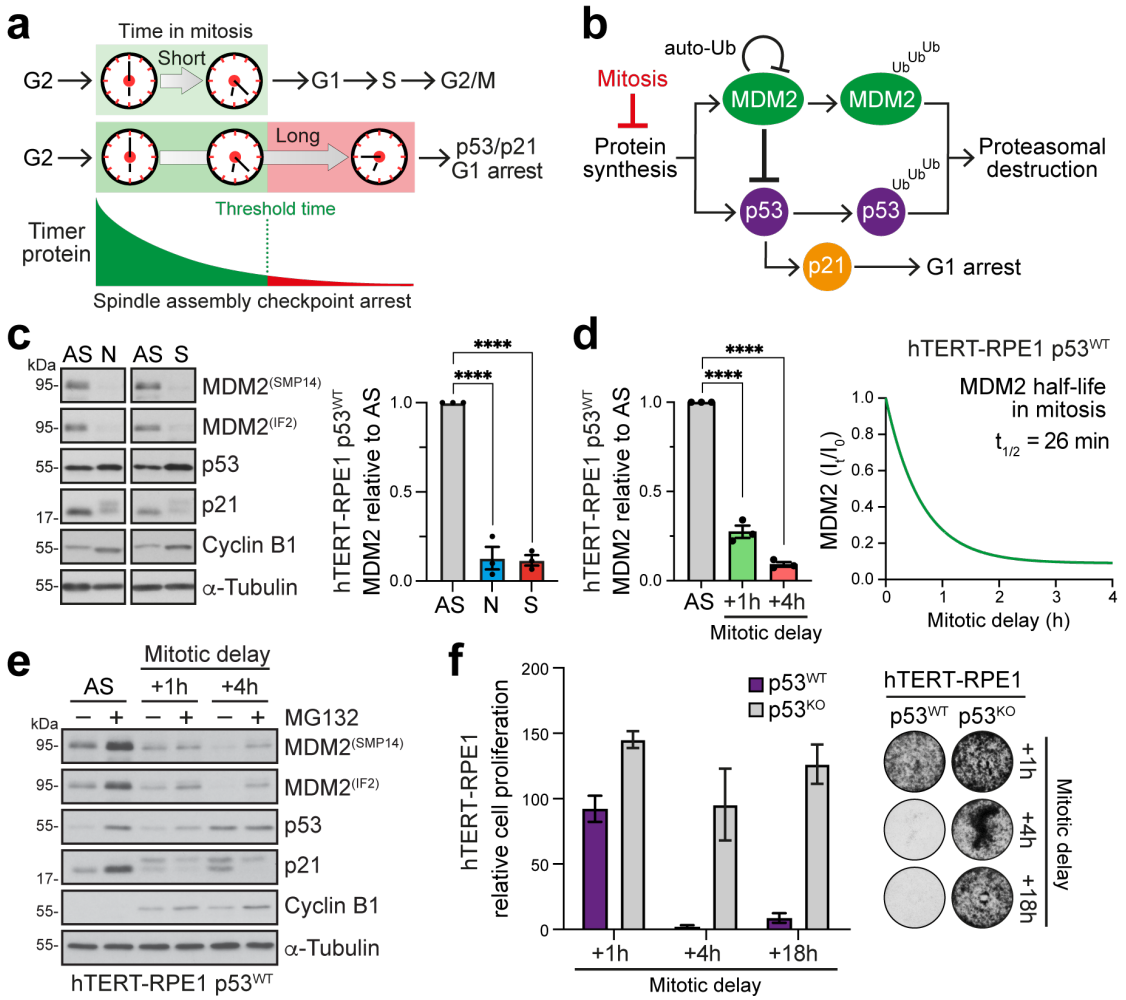

Fig. 1. The amount of MDM2 falls during mitosis and correlates with p53-dependent cell cycle arrest. a. A timer protein with a short half-life in mitosis could act as a sensor for the length of mitosis in the mitotic timer pathway. **b.** A schematic depicting MDM2 regulation of p53, and the role of ongoing protein synthesis and proteolysis in this pathway. **c.** The amount of MDM2 was measured by Western blotting in asynchronous (AS) or mitotic hTERT-RPE1 p53^{WT} cells, arrested in mitosis for 18 h with 100 ng/ml nocodazole (N) or 5 µM S-trityl L-cysteine (STLC, S) (mean ± SEM, n=3). **d.** The amount of MDM2 was measured by Western blotting in asynchronous (AS) or mitotic hTERT-RPE1 p53^{WT} cells, arrested for 1 or 4 h with 25 ng/ml nocodazole (mean ± SEM, n=3). Mitotic MDM2 half-life was calculated from the curve fit plotted on the right. **e.** As in d. except cells were treated ± 20 µM MG-132 to inhibit the proteasome. Inhibition of the proteosome in mitotic cells blocks MDM2 turnover. **f.** hTERT-RPE1 p53^{WT} or p53^{KO} cells were arrested for 1, 4 or 18 h with 25 ng/ml nocodazole. Mitotic cells were harvested, and 5000 cells plated per well. After 5 days cell proliferation was measured by crystal violet staining (mean ± SEM, n=3). Representative stained wells are shown.

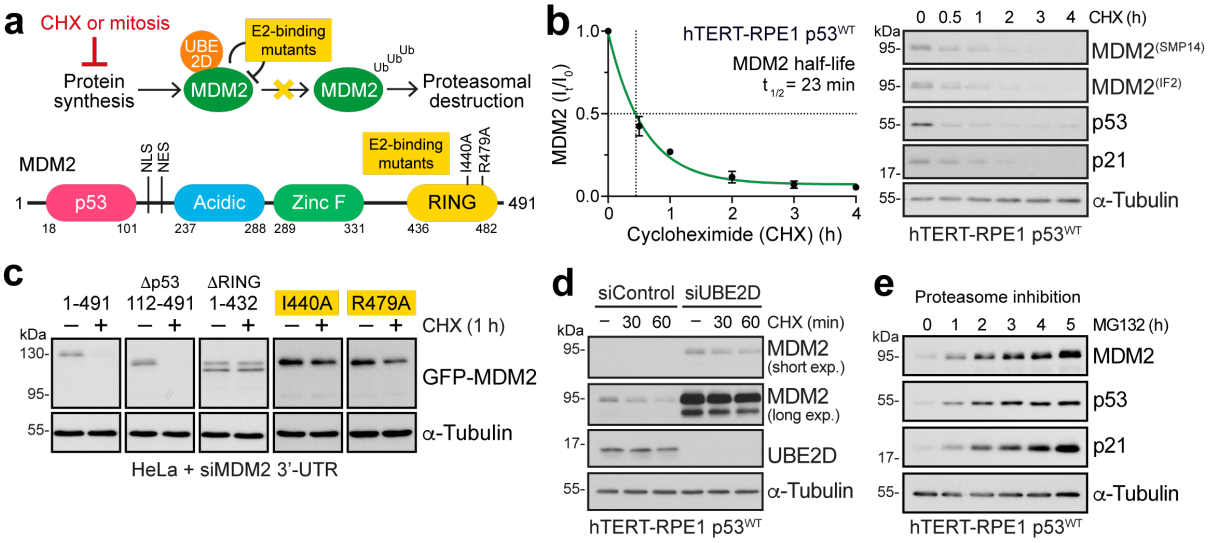

Fig. 2. MDM2 turnover requires the RING domain and is antagonised by USP7. a. A schematic depicting regulation of MDM2 by auto-ubiquitination (top). The domain structure of MDM2 is cartooned with two E2-binding mutants (bottom). **b.** MDM2 half-life was measured using Western blotting by adding solvent (–) or 50 µg/ml cycloheximide (CHX) to block protein synthesis, and then collecting samples up to 4 h. MDM2 half-life is indicated in the graph (mean ± SEM, n=3), with example Western blots. **c.** The stability of full-length GFP-MDM2 (1-491), and deletion or point mutant constructs was tested using 50 µg/ml cycloheximide (CHX) to block protein synthesis for 1 h (+). Solvent lacking cycloheximide was used as a control (–). **d.** The stability of endogenous MDM2 was tested in hTERT-RPE1 p53^{WT} cells, depleted of the MDM2 E2 enzymes UBE2D2/3 (siUBE2D), using 50 µg/ml CHX up to 1 h. Control non-targeting siRNA was used as a control. **e.** The amount of MDM2 was measured by Western blotting in cells treated for 0 to 5 h with 20 µM of the proteasome inhibitor MG-132.

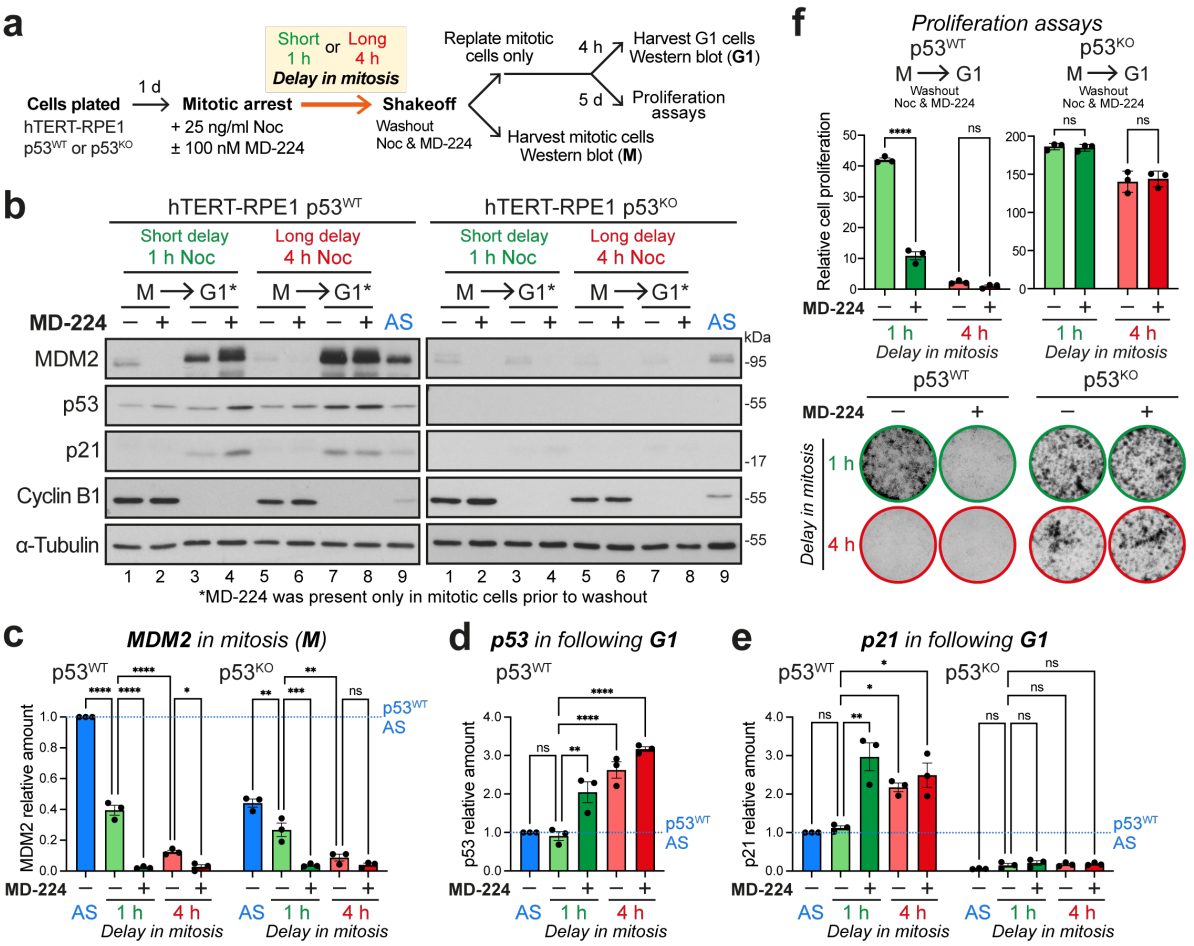

Fig. 3. Selective MDM2 destabilisation in mitosis results in p53-dependent p21 induction and reduced cell proliferation. a. A plan of the experimental design used for b-f. **b.** Western blot of cyclin B1 positive mitotic (M) and cyclin B1 negative (G1) hTERT-RPE1 $p53^{WT}$ or $p53^{KO}$ cells arrested for either 1 h or 4 h in mitosis with 25 ng/ml nocodazole, in the absence (–) or presence (+) of 100 nM MD-224 for the final hour (lanes 1-8). Samples from asynchronous hTERT-RPE1 $p53^{WT}$ and $p53^{KO}$ cells (AS) were loaded in the last lane to indicate the steady-state level of MDM2, p53 and p21 prior to entry into mitosis (lane 9). **c-e.** Graphs showing the relationship between the amount of MDM2 in mitosis (**c**), or p53 (**d**) and p21 (**e**) in the following G1 phase in $p53^{WT}$ and $p53^{KO}$ hTERT-RPE1 cells. Asynchronous hTERT-RPE1 $p53^{WT}$ cells (AS) were used as a normalisation control for the graphs to allow direct comparison of the steady-state levels of MDM2, p53 and p21 in $p53^{WT}$ and $p53^{KO}$ cells. **f.** Cell proliferation was measured for both hTERT-RPE1 $p53^{WT}$ or $p53^{KO}$ mitotic cells treated as in b, using colony formation assays (mean ± SEM, n=3).

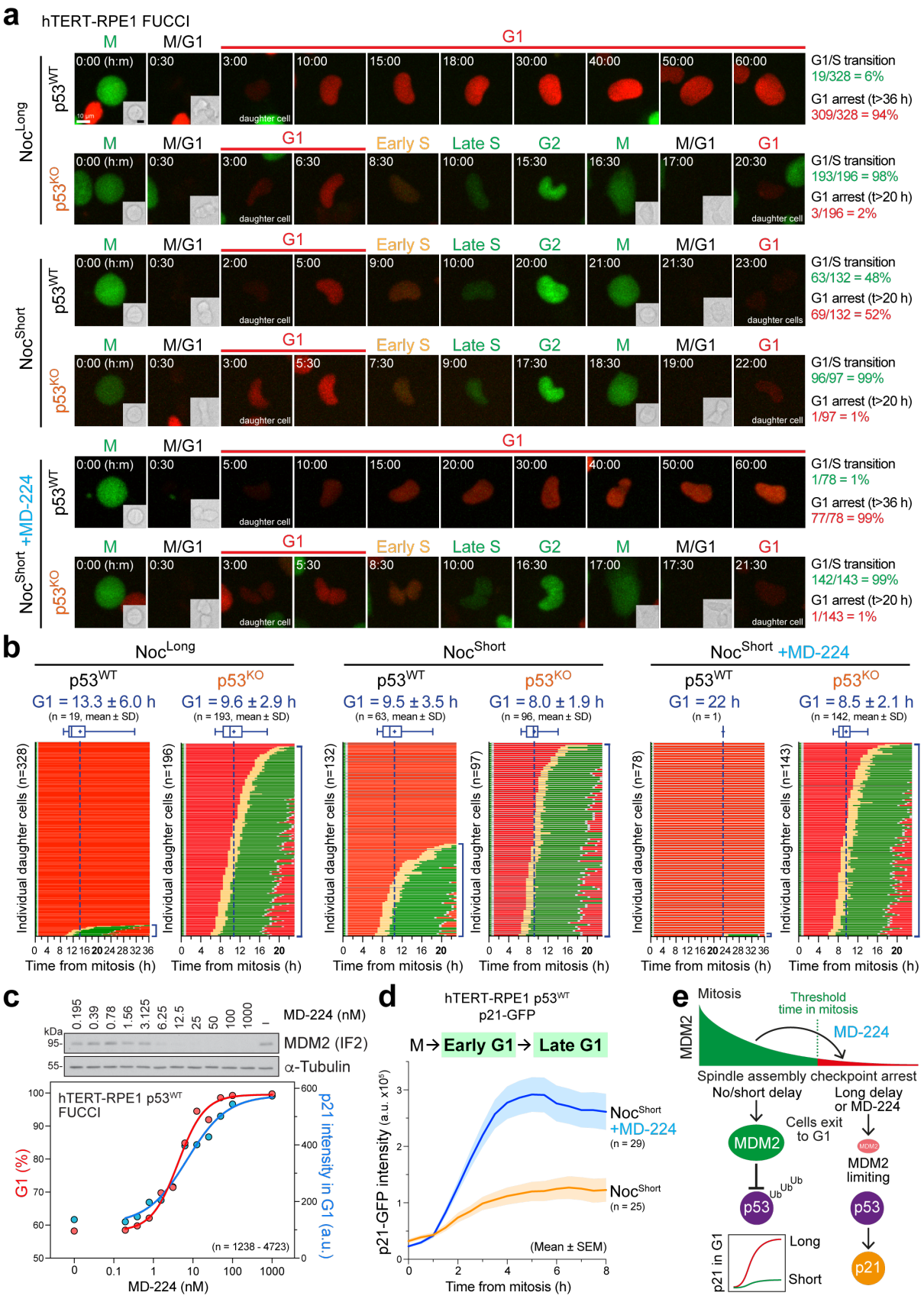

Fig. 4. MDM2 destabilisation in mitosis triggers robust cell cycle arrest in the following G1. a. Representative images of hTERT-RPE1 p53^{WT} and p53^{KO} FUCCI cells exiting mitosis and entering the following cell cycle following arrest in mitosis for either 30 min (Noc^{Short}) or 4 h (Noc^{Long}) with 25 ng/ml nocodazole, in the absence (–) or presence (+) of 100 nM MD-224 for 30 min prior to washout.

The mitotic cells were tracked after washout and imaged up to 60 h post-mitosis. The number and proportion of cells arresting in G1 and cells entering S phase are shown. **b.** Single cell traces of hTERT-RPE1 $p53^{WT}$ and $p53^{KO}$ FUCCI cells treated as in panel a. passing from mitosis into the following cell cycle. A red line indicates interphase, yellow early S-phase, green late S-, G2-phase and mitosis, and grey anaphase. The duration of G1 to cells entering S-phase is shown for all conditions (mean ± SD, sample sizes indicated in the figure). The dotted line in each panel of traces indicates the mean length of G1. A box and whiskers plot show the mean G1 length (+) and 95% confidence intervals. **c.** Titration of MD-224 to reveal the threshold concentration required for G1 arrest (red line) of hTERT-RPE1 $p53^{WT}$ FUCCI cells. MDM2 levels were determined by Western blotting, and p21 levels by immunofluorescence microscopy (blue line). **d.** Levels of p21 were followed in new G1 cells for the Noc^{Short} (n=25) and Noc^{Short}+MD-224 (n=29) conditions (mean ± SEM plotted on the graph). **e.** A schematic depicting how MDM2 levels drop in prolonged mitosis to a limiting level for p53 regulation in early G1, triggering p21 induction and cell cycle arrest.

345 **Supplemental Figures**

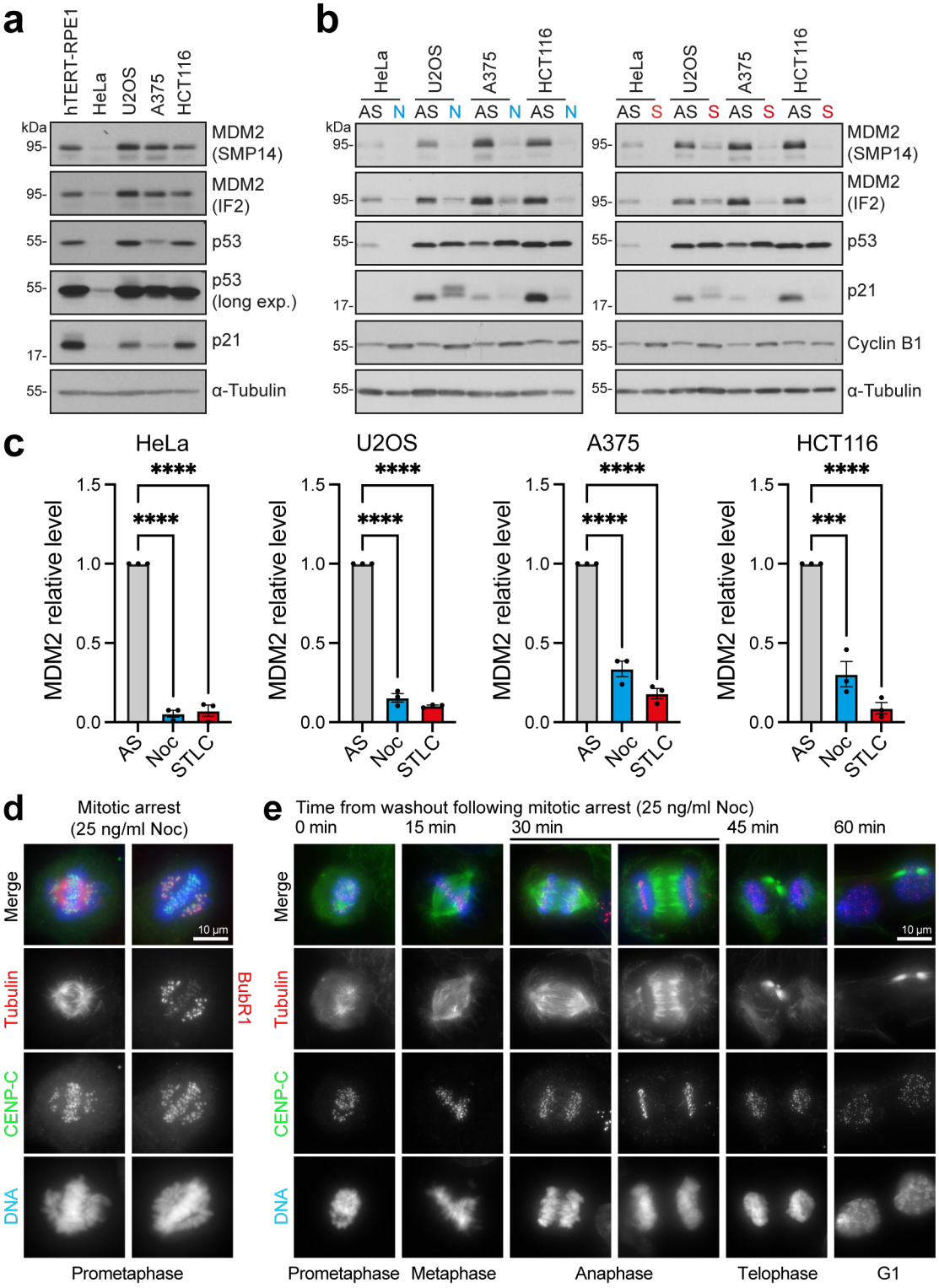

346

347 **Fig. S1. Reduction in the amount of MDM2 during mitosis in different human cell lines.**

348 **a.** The amounts of MDM2, p53 and p21 were measured in hTERT-RPE1 p53^{WT}, HeLa, U2OS, A375 and
349 HCT116 cell lines under standard culture conditions using Western blotting. α-Tubulin is a loading
350 control. **b.** The amount of MDM2 was measured by Western blotting in asynchronous (AS),
351 nocodazole (N) or S-trityl L-cysteine (STLC, S)-arrested mitotic HeLa, U2OS, A375 and HCT116 cell
352 lines. **c.** Quantification of MDM2 in HeLa, U2OS, A375 and HCT116 cell lines using data from b.
353 Values are expressed relative to the AS control for that cell line (mean ± SEM, n=3). **d.** hTERT-RPE1

354 cells treated with 25 ng/ml nocodazole (Noc) were fixed and stained for DNA, tubulin, the
355 kinetochore protein CENP-C or a spindle assembly checkpoint marker BubR1. **e.** Nocodazole was
356 removed by washing and cells imaged at the specified time points as they exit mitosis and enter G1.
357

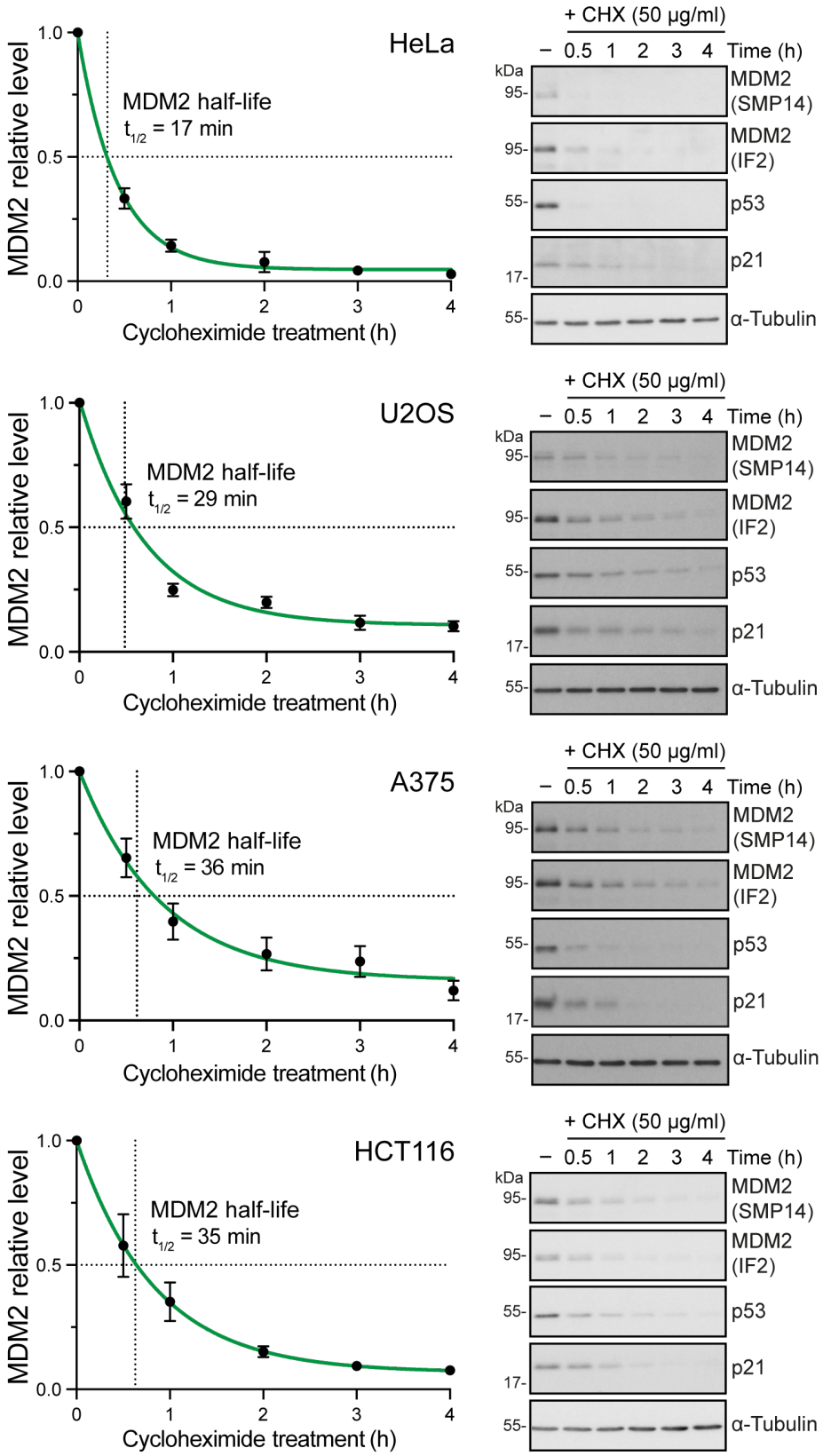

Fig. S2. Short half-life is a general property of MDM2 in multiple human cell lines. MDM2 half-life was measured in HeLa, U2OS, A375 and HCT116 cell lines by adding solvent (–) or 50 µg/ml cycloheximide (CHX) to block protein synthesis, and then collecting samples up to 4 h. MDM2 half-life is indicated in the graph (mean ± SEM, n=3), with example western blots.

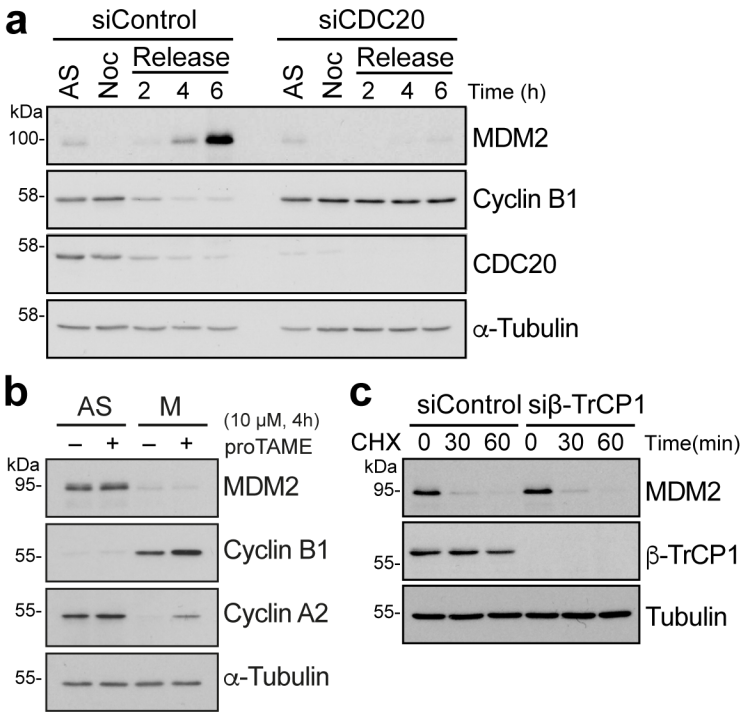

Fig. S3. APC/C^{CDC20} and SCF$^{\beta\text{-TRCP1}}$ do not regulate MDM2 stability in mitosis. a. Cells depleted of the APC/C co-activator CDC20 (siCDC20) or treated with a non-targeting control (siControl) were arrested in mitosis for 18 h with 25 ng/ml nocodazole (Noc). Nocodazole was washed out to test for CDC20 depletion, confirmed by cyclin B1 stabilisation for up to 6 h in the siCDC20 treated cells. Untreated asynchronous cells (AS) were taken as a control. Compared to asynchronous (AS) cells, MDM2 was lost during the mitotic arrest independently of CDC20, and did not recover in the washout in CDC20-depleted cells due to the sustained mitotic arrest. MDM2 recovered in the control cells due to resumption of protein synthesis during mitotic exit and G1 entry. **b.** MDM2 levels were measured in AS and 25 ng/ml nocodazole-arrested mitotic cells by Western blot after 4 h treatment with 10 μM of the APC/C inhibitor proTAME. **c.** MDM2 stability was measured by Western blot after 1 h treatment with 50 μg/ml cycloheximide (CHX) in cells depleted of the SCF subunit β-TRCP1. Non-targeting siRNA was used as a control.

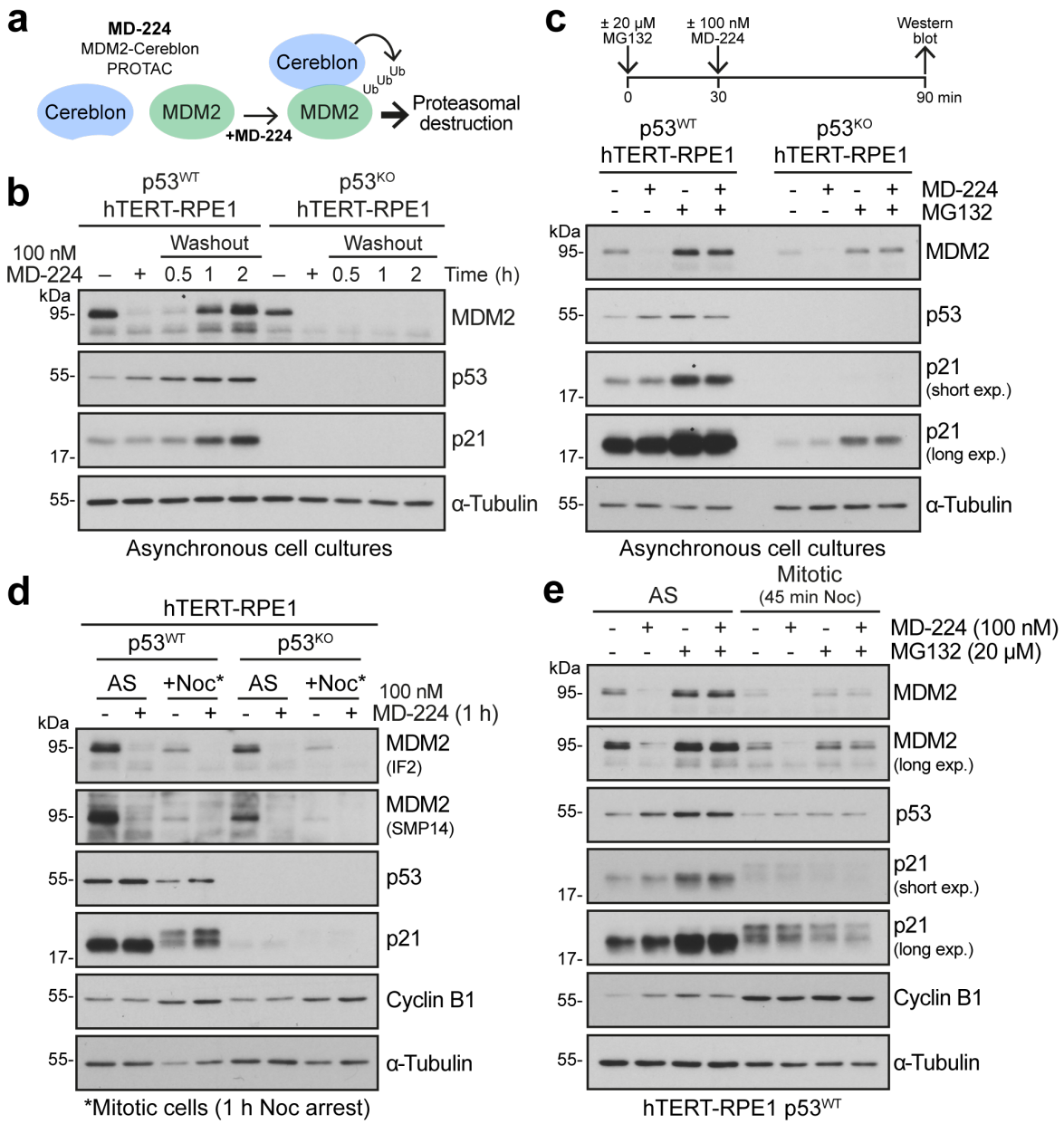

Fig. S4. MD-224 results in rapidly reversible MDM2 destruction in hTERT-RPE1 cells. a. A cartoon showing the mode of action for MD-224. **b.** hTERT-RPE1 p53^{WT} or p53^{KO} cells were treated with 100 nM MD-224 for 1 h (+) or a solvent control (–). MD-224 was then washed out with fresh growth medium for 0.5 to 2 h and Western blotted for MDM2, p53 and p21. Tubulin was used as a loading control. **c.** The amount of MDM2 was measured by Western blotting in asynchronous (AS) hTERT-RPE1 p53^{WT} and p53^{KO} cells treated for 90 min with (+) or without (–) the proteasome inhibitor MG132 (20 μM) and for 1 h with (+) or without (–) 100 nM MD-224. **d.** The amount of MDM2 was measured in asynchronous cells (AS) or mitotic hTERT-RPE1 p53^{WT} and p53^{KO} cells arrested for 1 h with 25 ng/ml nocodazole (+Noc) in the presence (+) or absence (–) of 100 nM MD-224. MDM2 was detected by Western blot using two different antibodies. **e.** The amount of MDM2 was measured using Western blotting in asynchronous cells (AS) or mitotic hTERT-RPE1 p53^{WT} cells arrested for 45 min with 25 ng/ml nocodazole (+Noc) in the presence (+) or absence (–) of 100 nM MD-224 and the proteasome inhibitor MG132 (20 μM).

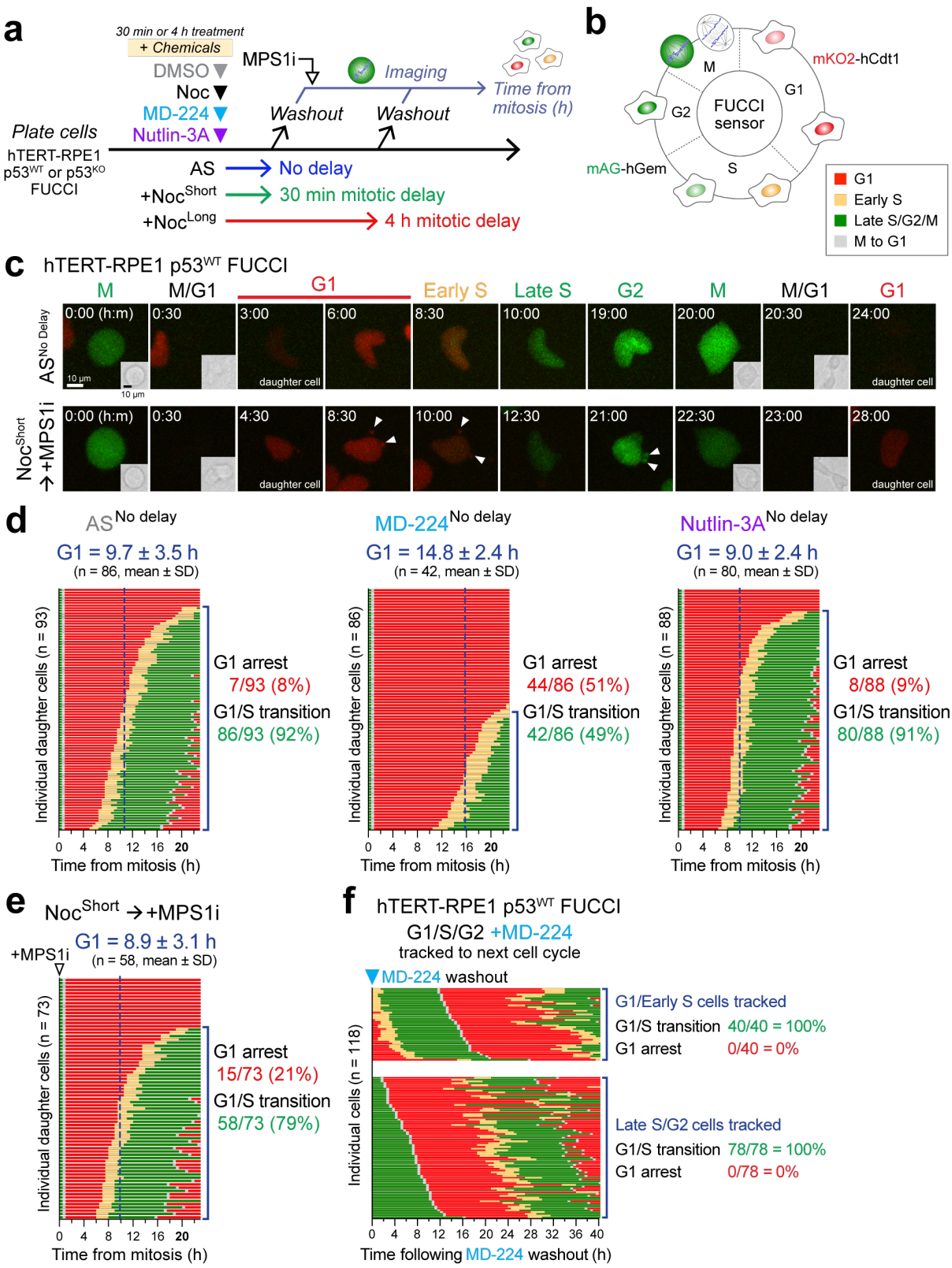

Fig. S5. hTERT-RPE1 FUCCI cell lines progress through G1 into S phase when mitosis is not delayed. **a.** Experimental design used for Figure 4. **b.** The properties of the FUCCI sensor. **c.** Representative images of hTERT-RPE1 p53^{WT} FUCCI from an asynchronous culture (AS) used as a control for an unperturbed cell cycle without any delay (AS$^{No\ delay}$), or a short delay followed by addition of MPS1 inhibitor (Noc^{Short} + MPS1i) to silence the spindle checkpoint and promote rapid mitotic exit. Arrowheads indicate micronuclei. **d.** Single cell traces of hTERT-RPE1 p53^{WT} FUCCI cells in AS$^{No\ Delay}$ (DMSO$^{No\ delay}$) (n = 93), MD-224$^{No\ delay}$ (n = 86) or Nutlin-3A$^{No\ delay}$ (n = 88) treated conditions passing

401 from mitosis into the following cell cycle. **e.** Single cell traces of hTERT-RPE1 p53^{WT} FUCCI cells in the
402 Noc^{Short} + MPS1i (n = 73) condition passing from mitosis into the following cell cycle. The duration of
403 G1 in cells entering S-phase is shown (mean ± SD). The dotted line in each panel of traces indicates
404 the mean length of G1. The number and proportion of cells arresting in G1 and cells entering S phase
405 are indicated. **f.** Single cell traces of hTERT-RPE1 p53^{WT} FUCCI cells in either G1/S or S/G2 in
406 asynchronous cultures were treated with MD-224 as in the Noc^{Short} condition, washed to remove the
407 drug, then tracked into the following cell cycle. The proportion of cells arresting in G1, entering S
408 phase, and duration of G1 in cells entering S-phase are shown (mean ± SD, n = 118).
409

410 **Materials and methods**

411 Reagents and antibodies

412 General laboratory chemicals were obtained from Merck, Sigma-Aldrich, and Thermo Fisher
413 Scientific. Commercially available polyclonal antibodies (pAbs) or monoclonal antibodies (mAbs)
414 used for Western blotting (WB) and immunofluorescence (IF), and are listed in Table 1.

415

Antibody target	Company	mAb/pAb?	Catalogue number	Species	Dilution (WB)	Dilution (IF)
MDM2 (IF2)	Millipore	mAb	OP46	Mouse	1:1000	
MDM2 (SMP14)	Abcam	mAb	Ab3110	Mouse	1:1000	
MDM2 (D1V2Z)	CST	mAb	86934	Rabbit	1:1000	
p53 (DO-7)	CST	mAb	48818	Mouse	1:1000	1:1000
p21 (12D1)	CST	mAb	2947	Rabbit	1:1000	1:1000
UBE2D3/UbcH5C (D60E2)	CST	mAb	4330	Rabbit	1:1000	
Cyclin B1 (GSN3)	Millipore	mAb	8A5D12	Mouse	1:5000	
Cyclin A2 (E399)	Abcam	mAb	Ab32498	Rabbit	1:500	
α-Tubulin (DM1A)	Sigma	mAb	T6199	Mouse	1:10,000	
Cdc20	Proteintech	pAb	10252-1-AP	Rabbit	1:1000	
β-TrCP (D13F10)	CST	mAb	4394	Rabbit	1:1000	
GFP (7.1 and 13.1)	Roche	mAb	11814460001	Mouse	1:1000	
FLAG®-HRP (M2)	Sigma-Aldrich	mAb	A8592	N/A	1:5000	
Vinculin (hVIN-1)	Sigma-Aldrich	mAb	V9264	Mouse	1:10,000	
yH2A.X pS139 (2F3)	BioLegend	mAb	613401	Mouse	1:1000	1:1000
Mouse-HRP	Jackson	pAb	715-035-150	Donkey	1:5000	
Rabbit-HRP	Jackson	pAb	711-035-152	Donkey	1:5000	
Anti-Rabbit AlexaFluor®-488	Thermo Fisher	pAb	A21206	Donkey		1:1000
Anti-Mouse AlexaFluor®-568	Thermo Fisher	pAb	A10037	Donkey		1:1000

416 Table 1: Primary and secondary antibodies used in this study.

417

418 Inhibitors and drug compounds

419 Commercially-sourced inhibitors or drug compounds used in this study, and the solvents used to
420 reconstitute them, are listed in Table 2. Experiment-specific timings and concentrations are given in
421 the figure legends.

422

Drug/inhibitor	Target	Company	Catalogue #	Concentration	Solvent
Nocodazole	Microtubules	Sigma-Aldrich	487928	25 or 100 ng/ml	DMSO
STLC	KIF11	Sigma-Aldrich	164739	5 µM	DMSO
MD-224	MDM2	MedChemExpress	HY-114312	100 nM	DMSO
Nutlin-3a	MDM2/p53 interface	Selleck Chem	S8059	2.5 µM	DMSO
Cycloheximide	Ribosome	Sigma-Aldrich	C7698	50 µg/ml	Water
MG132	Proteasome	Sigma-Aldrich	474790	20 µM	DMSO
AZ3146	MPS1	TOCRIS	3994	2 µM	DMSO
proTAME	APC/C	BostonBiochem	I-440	10 µM	DMSO
Hydroxyurea	Ribonucleotide reductase	Sigma-Aldrich	H8627	2 mM	Water

423 Table 2: small molecules used in this study.

424

425 MDM2 expression plasmid construction

426 Mammalian eGFP-MDM2 expression plasmids were generated using pEF5/FRT or pcDNA5/FRT
427 plasmids harbouring eGFP followed by a 25 amino acid linker YK$(GSSS)_5$RIP 5' to the multiple cloning
428 site, as the backbone. The full-length MDM2 coding sequence was isolated from Addgene plasmid
429 #16233 (pcDNA3 FRT MDM2) by PCR using the KOD hot start polymerase kit (Merck #71086), using
430 primers that included a 5' BamHI restriction site, and a 3' XhoI restriction site. Following BamHI (NEB
431 #R3136)-XhoI (NEB #R0146) digest of the MDM2 PCR product and destination vector, ligations were
432 performed with T4 ligase (NEB #M0202). Ligated plasmids were transformed into competent XL-1
433 blue cells (Agilent Technologies #200249). I440A and R479A MDM2 mutants were generated by site-
434 directed mutagenesis, using KOD polymerase (Merck #71086). MDM2 truncated fragments were
435 generated by PCR using Addgene plasmid #16233 (pcDNA3 FRT MDM2) as a template and cloned
436 into pEF5 FRT eGFP with BamHI-XhoI. Primers used to generate constructs, are listed in Table 3.

437

Construct	Forward Primer	Reverse primer
MDM2	N/A	N/A
$MDM2^{112\text{-}end}$	GGGGGATCCCCATGCAGCAG GAATCATCGGACTCAG	GGGCTCGAGCTAGGGGAAAT AAGTTAGCACAATCATTTG
$MDM2^{1\text{-}432}$	GGGGGATCCGCCACCATGTG CAATACCAACATGTCTGTACC	GGGCTCGAGCTAAAGGGGC AAACTAGATTCCACACTC
$MDM2^{112\text{-}432}$	GGGGGATCCCCATGCAGCAG GAATCATCGGACTCAG	GGGCTCGAGCTAAAGGGGC AAACTAGATTCCACACTC
$MDM2^{I440A}$	CATTGAACCTTGTGTGGCTTG TCAAGGTCGACC	GGTCGACCTTGACAAGCCAC ACAAGGTTCAATG
$MDM2^{R479A}$	GCCCTGCCCAGTATGTGCCCA ACCAATTCAAATG	CATTTGAATTGGTTGGGCAC ATACTGGGCAGGGC

438 Table 3: MDM2 plasmids generated in this study.

439

440 Cell lines and cell culture

441 hTERT-RPE1 cells (#CRL-4000) were purchased from ATCC and cultured in DMEM-F12 Ham medium
442 (Sigma #D6421), supplemented with GlutaMAX™ (Gibco #35050087) and 10% (v/v) fetal bovine
443 serum (FBS, Sigma-Aldrich #F9665). HeLa S3 (#CRL-2.2), A375 (#CRL-1619), U2OS (#HTB-96), and
444 HEK293T (#CRL-3216) cells were purchased from ATCC and cultured in DMEM containing
445 GlutaMAX™ (Gibco #10569010) and 10% (v/v) FBS. HCT116 cells (#CCL-247) were purchased from
446 ATCC and cultured in McCoy's 5A medium (Gibco #16600082), supplemented with 10 mM sodium
447 pyruvate (Thermo Fisher #11360088) and 10% (v/v) FBS. For routine passaging of cells, cells were
448 washed in PBS, and incubated with TrypLE™ Express Enzyme cell dissociation reagent (Gibco
449 #12605036) for 5 min at 37°C, before resuspending detached cells in full medium for passage. All cell
450 lines are wild-type for p53. HeLa cells express the HPV E6/E7 proteins which result in p53
451 downregulation. All cell lines were maintained in a humidified 37°C cell culture incubator (Thermo,
452 HERAcell, #51013568), at 5% (v/v) CO_2.

453

454 Transient transfection of cells

455 Cells were seeded at a density of 50,000 cells per well in 6-well plates. The next day, transfection
456 mixes were prepared in sterile DNase-free Eppendorf tubes (Eppendorf #0030108035) consisting of
457 100 µl Opti-MEM (Gibco #11058021), 3 µl Mirus TransIT-LT1 transfection reagent (Mirus #MIR2300),
458 and up to 1 µg of plasmid DNA. If less than 1 µg plasmid DNA was required, carrier pBlueScript II
459 (Agilent) empty plasmid was used to bring the total amount of DNA up to 1 µg. Transfection mixes
460 were vortexed briefly for 20 s, and incubated at room temperature for 30 min, before adding drop-
461 wise to cells. Cells were then left to grow for the times indicated in the figure legends.

462

463 CRISPR/Cas9 gene editing of hTERT-RPE1 cells

464 First, hTERT-RPE1 cells were edited to create a functionally null puromycin resistance cassette
465 through delivery of two pX461 vectors (Addgene #48140) containing the appropriate guide RNA
466 (gRNA) sequence (Table 4) using the Amaxa™ nucleofector™ kit V (Lonza #VCA-1003). Monoclonal
467 lines were screened for puromycin sensitivity, growth rate, and cilium formation. We refer to this
468 cell line as hTERT-RPE1 $p53^{WT}$ throughout. Subsequently, to generate p53 knockout cells, the pX459
469 vector containing guide RNA against p53 (CCATTGTTCAATATCGTCCGGGG) was delivered through
470 electroporation. After brief selection in puromycin, monoclonal lines were screened for Nutlin-3a
471 resistance, followed by extensive quality controls including immunoblotting and amplification of the
472 targeted genomic region by PCR. Genomic DNA was isolated from clones using QuickExtract™ DNA
473 isolation solution (Lucigen #QE09050). PCRs were performed with KOD hot-start polymerase (Merck
474 #71086), using primers flanking the gRNA recognition site. PCR products were ligated into pSC-A
475 vectors using a Blunt-end PCR cloning kit (Agilent #240207). Ligated plasmids were transformed into
476 XL-1 blue competent cells, and around 10 colonies were mini-prepped (Qiagen #27107) and
477 sequenced using Sanger DNA sequencing (Source Genomics, Cambridge, UK) in order to cover all
478 edited alleles. The $p53^{KO}$ cell lines were STR profiled using the ATCC cell line authentication service
479 (ATCC, Manassas, VA), and validated as hTERT-RPE1. We refer to this cell line as hTERT-RPE1 $p53^{KO}$
480 throughout.

481

482 hTERT-RPE1 FUCCI cell line generation

483 The hTERT-RPE1 $p53^{WT}$ and $p53^{KO}$ FUCCI cells used here were generated by lentiviral infection.
484 Briefly, pBOB-EF1-FastFUCCI-Puro (Addgene, #86849), pMD2.G (Addgene #12259) and psPAX2
485 (Addgene #12260) (gifts from Didier Trono) were used for lentiviral-based packaging in HEK293T
486 cells for two days with a media change after 24 h. The resulting lentiviral supernatant was used to
487 infect hTERT-RPE1 $p53^{WT}$ and $p53^{KO}$ for 24 h. After infection, antibiotic-resistant clones were selected

488 by puromycin and then expanded in non-selective medium to be screened by fluorescence
489 microscopy for successful integration of the FUCCI sensor.
490
491 RNA interference
492 Cells were seeded at a density of 50,000 cells per well in 6-well plates. The next day, transfection
493 mixes were prepared in sterile DNase-free Eppendorf tubes consisting of 100 µl Opti-MEM (Gibco
494 #11058021), and either 3 µl Mirus TransIT-X2 transfection reagent (Mirus #MIR6000) for hTERT-
495 RPE1 cells, or 3 µl Oligofectamine (Thermo #12252011) for HeLa cells. Solutions were mixed and
496 incubated for 5 min at room temperature, then 60 pM siRNA was added, followed by incubation at
497 room temperature for 30 min, before adding drop-wise to cells. Cells were left to grow for the times
498 indicated in the figure legends. siRNAs used in this study are listed in Table 4.
499

siRNA	Source	Catalogue # or sequence
siβ-TrCP1 SMARTpool	Dharmacon	L-003463-00-0005
siCDC20 SMARTpool	Dharmacon	L-003225-00-0005
siGL2 luciferase control	Dharmacon	D-001100-01-50
siMDM2 3'–UTR	Dharmacon	J-003279-13-0005

500 Table 4: siRNA information for the siRNA sequences used in this study.
501
502 Mitotic timer assays
503 For mitotic timer assays, hTERT-RPE1 $p53^{WT}$ or $p53^{KO}$ cells were seeded into 10-cm dishes (five dishes
504 per condition) for 80% confluency the next day. The next day, cells were treated with 25 ng/ml
505 nocodazole for 45 min at 37°C. Mitotic cells were isolated by shake-off, and washed three times in
506 pre-warmed 37°C full medium (with pelleting performed at 200 × g for 3 min at 37°C in between
507 washes) before lysing 50% (w/v) of the cells for a mitotic sample, and re-plating the other 50% (w/v)
508 of the cells for 4 h at 37°C for a G1 sample. Alternatively, following mitotic shake-off, cells were
509 pelleted and re-suspended in full medium containing 25 ng/ml nocodazole and re-plated into 6-cm
510 dishes for longer mitotic samples. Following the longer mitotic arrests, cells were isolated by shake-
511 off, and washed three times in pre-warmed 37°C full medium (with pelleting performed at 200 × g
512 for 3 min at 37°C in between washes) before lysing 50% (w/v) of the cells for a mitotic sample, and
513 re-plating the other 50% (w/v) of the cells for 4 h at 37°C for a G1 sample. Where indicated, MD-224
514 or DMSO (Sigma #D8418) vehicle control was added in the last 45 min of mitosis, before the
515 nocodazole washout procedure. Asynchronous cells were used as controls, and were treated with
516 MD-224 or DMSO vehicle control for the same time as in the mitotic conditions. AS control cells
517 were either lysed after the treatment time, or washed three times in pre-warmed 37°C full medium
518 and incubated in fresh full medium at 37°C for 4 h, for a washout control.
519
520 Cell lysis for Western blots
521 Following treatments, cells were moved to ice and washed in ice-cold PBS. PBS was removed and
522 cells were lysed in lysis buffer (20 mM Tris-HCl (Sigma-Aldrich, #T4661) pH 7.4, 150 mM NaCl
523 (Sigma-Aldrich #S3014), 1% (v/v) IGEPAL (Sigma-Aldrich #S3014), 0.1% (w/v) sodium deoxycholate
524 (Sigma-Aldrich #D6750), 40 mM sodium β-glycerophosphate (Sigma-Aldrich #G9422), 10 mM NaF
525 (Sigma-Aldrich #201154), 0.3 mM sodium orthovanadate (Sigma-Aldrich #S6508), 100 nM okadaic
526 acid (Enzo Life Sciences #ALX-350-011-M001), 200 nM microcystin-LR (Enzo Life Sciences #ALX-350-
527 012-M001), 1 mM DTT (Sigma-Aldrich #11583786001), 1× protease inhibitor cocktail (Roche,
528 cOmplete™, EDTA-free Protease Inhibitor Cocktail, #11873580001), and 1× phosphatase
529 inhibitor cocktail (Sigma, P0044) in water). Lysates were harvested, moved to 1.5-ml Eppendorf
530 tubes (Eppendorf #10451043), and incubated on ice for 10 min. Lysates were then clarified at

531 14,000 rpm for 15 min at 4°C. Protein concentrations were measured by Bradford assay using
532 Protein Assay Dye Reagent Concentrate (Bio-Rad, 5000006). Samples were normalised to 0.5-1
533 mg/ml. Sample buffer (0.1875 mM Tris-HCl (Sigma-Aldrich, #T4661) pH 6.8, 1% (w/v) SDS (Sigma-
534 Aldrich #75746), 10% (v/v) glycerol (Sigma-Aldrich #G9012), 0.05% (w/v) bromophenol blue (Sigma-
535 Aldrich #B5525), and 10% (v/v) β-mercaptoethanol (Sigma-Aldrich #M3148) in water) was added,
536 and samples were boiled at 95°C for 10 min, before progressing to SDS-PAGE and Western blotting.
537

538 SDS-PAGE and Western blotting

539 Proteins were separated by SDS-PAGE (Bio-Rad, Mini-PROTEAN® Tetra cell, #1658000) and
540 transferred onto nitrocellulose membranes (Bio-Rad #1704158, #1704159) using a Trans-blot Turbo
541 system (Bio-Rad #1704150). After transfer, blots were blocked in 5% (w/v) milk powder in PBS
542 (PanReac AppliChem #A0965,9100)-TWEEN® 20 (Sigma-Aldrich #P1379) (PBS-T), before incubation
543 with primary antibodies (Table 1) diluted in 5% (w/v) milk in PBS-T for 1 h at room temperature, or
544 at 4°C overnight. Blots were then washed in PBS-T before incubating with the secondary HRP-
545 conjugated antibodies (Table 1) for 1 h at room temperature, before washing again in PBS-T. Signals
546 were revealed using ECL (GE Healthcare #RPN2106) and visualised on X-ray films (GE Healthcare
547 #GE28-9068-37), developed on an OPTIMAX 2010 X-ray Film Processor (PROTAC-Med).
548

549 Cell proliferation assays

550 To test for proliferation, hTERT-RPE1 $p53^{WT}$ or $p53^{KO}$ cells as described in the figures were treated as
551 described in the mitotic timer assays methods section. Following nocodazole washout, mitotic cells
552 were counted using a Neubauer chamber and were seeded at 5,000 cells per well in 6-well plates.
553 Cells were cultured at 37°C for five days. Following incubation, cells were washed in PBS and
554 fixed/stained in crystal violet/methanol solution (25% (v/v) methanol (VWR #20847.307) + 5% (w/v)
555 crystal violet (Sigma-Aldrich #C0775) in water) for 30 min at room temperature. The crystal violet
556 stain was then removed, and cells washed in water. Plates were left to dry on top of a piece of
557 Whatman paper before imaging on a Bio-Rad Gel Doc XR+ imaging system (Bio-Rad, 1708195EDU).
558 hTERT-RPE1 cells are highly mobile and do not form distinct colonies. The extent of cell proliferation
559 was assessed using densitometry on Fiji/Image J software (National Institutes of Health).
560

561 Cell-cycle tracking using hTERT-RPE1 $p53^{WT}$ and $p53^{KO}$ FUCCI cell lines

562 For single cell tracking, cells were plated in 35-mm dishes with a 14-mm 1.5 thickness cover glass
563 window on the bottom (MatTek Corp, P35G-1.5-14-C). For imaging, the dishes were placed in a 37°C
564 and 5% CO_2 environment chamber (Tokai Hit) on the microscope stage. Imaging was performed on
565 an Ultraview Vox spinning disk confocal system running Volocity software (PerkinElmer) using the
566 20×/0.75 NA UPlanSApo objective on an Olympus IX81 inverted microscope equipped with an
567 electron multiplying charge coupled device (EM-CCD) camera (C9100-13, Hamamatsu Photonics).
568 Cells were excited by 488 nm and 561 nm lasers with 200 ms exposures at 3-6% laser power.
569 Brightfield reference images were also taken to visualize cell shape with 30 ms exposures. 12-µm
570 image stacks with intervals of 0.6 µm (total 21 planes) were collected at the time intervals indicated
571 in the figures and then maximum intensity projected and cropped in Fiji/Image J (National Institutes
572 of Health) for further analysis. Before the imaging, cells were treated with either 0.1% (v/v) DMSO as
573 a control, 25 ng/ml (82.5 nM) nocodazole, 100 nM MD-224, or combinations of these chemicals for
574 30 min or 4 hours at 37°C, 5% CO_2 and then washed five times in pre-warmed 37°C full medium.
575 After the washout, the dish was immediately placed on the microscope, and then the mitotic cells
576 expressing mAG-hGem, in prometaphase or metaphase, were imaged and tracked to measure G1
577 duration.
578

579 Immunofluorescence microscopy

580 Cells plated on glass coverslips were washed in PBS, and fixed with 3% (w/v) PFA (Sigma-Aldrich
581 #158127) in PBS pH 7.4 at room temperature for 15 min. Unreacted PFA was quenched by washing
582 with 50 mM NH_4Cl (Sigma-Aldrich #213330) in PBS, following by a 10-min incubation in 50 mM NH_4Cl
583 in PBS. Cells were washed three times in PBS, followed by permeabilization with 0.2% (v/v) Triton™
584 X-100 (Sigma-Aldrich #X100) in PBS at room temperature for 5-10 min. Permeabilised cells were
585 washed three times in PBS before incubating with the appropriate primary antibodies (Table 1).
586 Antibody dilutions were performed in PBS, and coverslips were placed cell-side down on droplets of
587 antibody solutions, inside a humidified chamber for 1 h at room temperature. Following incubation,
588 cells were washed three times in PBS, and incubated with the secondary AlexaFluor-conjugated
589 antibodies (Table 1) for 1 h at room temperature, as described for the primary antibody incubation.
590 DAPI (Sigma-Aldrich #D9542) was added at the same time as the secondary antibodies, in order to
591 stain DNA. Following incubation, cells were washed three times in PBS, and once in water, before
592 mounting onto glass microscopy slides with Mowiol® 4-88 (Sigma-Aldrich #81381). Samples were
593 imaged on a standard upright microscope system (BX61, Olympus) with filter sets for DAPI,
594 GFP/Alexa Fluor 488, Cy3/Alexa Fluor 555 and Cy5/Alexa Fluor 647 (Chroma Technology Corp.), a
595 2048 × 2048-pixel complementary metal oxide semiconductor camera (Prime, Photometrics), and
596 MetaMorph 7.5 imaging software (Molecular Devices). Illumination was provided by an LED light
597 source (pE300, CoolLED Illumination Systems). Image stacks with a spacing of 0.4 µm through the
598 cell volume were maximum intensity projected and cropped in Image J (National Institutes of
599 Health).

600

601 Statistical analysis

602 Statistical analysis was performed using GraphPad Prism 9.3.1 (GraphPad Software). Statistical
603 significance was analysed using an unpaired two-tailed t-test with Welch's correction, a one-way
604 ANOVA, a Brown-Forsythe ANOVA, a Kruskal-Wallis test, or Dunn's multiple comparison test. Graphs
605 display the mean ± SD or SEM. P-values are shown on graphs as follows: $p \geq 0.05$ = not significant
606 (ns), $p < 0.05$ = *, $p < 0.01$ = **, $p < 0.001$ = ***, $p < 0.0001$ = ****.